CROATICA CHEMICA ACTA
CCACAA, ISSN 0011-1643, e-ISSN 1334-417X
Croat. Chem. Acta **84** (2) (2011) 259–268.
CCA-3473

Original Scientific Article

Human Dipeptidyl Peptidase III: the Role of Asn406 in Ligand Binding and Hydrolysis†

Jasminka Špoljarić,[a] Antonija Tomić,[b] Bojana Vukelić,[a] Branka Salopek-Sondi,[c] Dejan Agić,[d] Sanja Tomić,[b] and Marija Abramić[a,*]

[a]*Division of Organic Chemistry and Biochemistry, Ruđer Bošković Institute, Bijenička cesta 54, 10002 Zagreb, Croatia*
[b]*Division of Physical Chemistry, Ruđer Bošković Institute, Bijenička cesta 54, 10002 Zagreb, Croatia*
[c]*Division of Molecular Biology, Ruđer Bošković Institute, Bijenička cesta 54, 10002 Zagreb, Croatia*
[d]*Department of Chemistry, Faculty of Agriculture, The Josip Juraj Strossmayer University, Trg Sv. Trojstva 3, 31107 Osijek, Croatia*

RECEIVED DECEMBER 1, 2010; REVISED MAY 25, 2011; ACCEPTED JULY 18, 2011

Abstract. Human dipeptidyl peptidase III (DPP III) is a member of the zinc-metallopeptidase family M49 with a role in intracellular protein catabolism. Ligand-free crystal structure of yeast and human orthologues provided insight into the enzyme's active center and enabled some assumptions about the enzyme - substrate interactions. The molecular modeling performed for human and yeast DPP III indicated involvement of Asn406 and Asn415, respectively in ligand binding. To investigate further the role of this asparagine residue, conserved in all eukaryotic M49 peptidases, a site-directed mutagenesis of human DPP III was carried out. Replacement of Asn406 with Gln, but not with Ser, resulted in a large decrease in the enzyme's binding affinity for competitive peptide inhibitor and in catalytic efficiency. Molecular dynamics simulations performed for enzyme-substrate complexes, revealed changed coordination of the active-site zinc ion and the orientation of the catalytically important His568, in N406Q, but not in the N406S complexes.(doi: 10.5562/cca1808)

Keywords: dipeptidyl peptidase III, molecular dynamics, peptidase family M49, protein structure-function, site-directed mutagenesis

INTRODUCTION

Dipeptidyl peptidases (DPPs) cleave dipeptides from the (poly)peptides amino termini. In mammalian tissues originally four types of dipeptidyl peptidases, DPP I to IV have been recognized through hydrolysis of distinct synthetic substrates (unsubstituted dipeptidyl 2-naphthylamides) and extensively characterized.[1] Dipeptidyl peptidase III (DPP III; EC 3.4.14.4) is a widely-distributed cytosolic enzyme which selectively hydrolyses arginyl-arginyl-2-naphthylamide (Arg_2-2NA).[2] It was at first isolated and biochemically characterized from several human (placenta, erythrocytes, seminal plasma) and animal (bovine pituitary gland and adrenal medulla, porcine spleen, rat and guinea pig brain) tissues[3–11] as monomeric acidic metalloexopeptidase ($M_r \approx$ 80 000, pI ≈ 4.5) with a broad specificity whose optimally sized substrates are tetra- to octapeptides.[5,10] The same type of enzyme was partially purified and described from two lower eukaryotes, the slime mold *Dictyostelium discoideum* and the yeast *Saccharomyces cerevisiae*.[12,13] The physiological substrates of DPP III are mostly unknown, although it hydrolyzes a number of biologically active peptides *in vitro*. Besides its contribution in the final steps of intracellular protein catabolism, a regulatory role for DPP III was suggested.[5,9] High concentrations of DPP III in the rat spinal cord and its high affinity towards opioid peptides enkephalins and endomorphins imply its role in the mammalian pain-modulatory system.[14,15] Enhanced level of human DPP III activity and protein was found in endometrial carcinomas and in ovarian malignant neoplasms,[16] moreover correlation of DPP III activity and aggressiveness of ovarian primary carcinomas was shown.[17] It was proposed that DPP III, with several other endogenous peptidases in the lens plays an important role in cataractogenesis by inducing lens opacification through the intracellular turnover of lens proteins.[18] Recently, upregulated DPP III was identified as a proteomic biomarker for prenatal bisphenol A-exposure in mouse

† This article belongs to the Special Issue *Chemistry of Living Systems* devoted to the intersection of chemistry with life.
* Author to whom correspondence should be addressed. (E-mail: abramic@irb.hr)

Table 1. Primers used for site-directed mutagenesis of human DPP III cDNA

Mutant	Nucleotide sequence (5'−3') Primer I	Nucleotide sequence (5'−3') Primer II
N406S	gcagacggaaggctttaagtctgtgtcgctgggg	ccccagcgacacagacttaaagccttccgtctgc
N406Q	gcagacggaaggctttaagcaggtgtcgctgggg	ccccagcgacacctgcttaaagccttccgtctgc

Codons for the mutated residues are underlined.

immune organs.[19] The first DPP III amino acid sequences determined have been rat (738 amino acids) and human (737 amino acids), both possessing the characteristic HELLGH motif that resembles the HExxH one present in many metallopeptidases.[2,20] Fukasawa *et al.* demonstrated by atomic absorption spectrometry that both the recombinant rat DPP III and the natural human placental enzyme contain about one Zn^{2+} ion per molecule.[20] The flow of data on complete genome sequences in the last decade enabled recognition of dipeptidyl peptidase III family (peptidase family M49) as a distinct group of metallopeptidases, based on their sequence relationships and the unique hexapeptide motif HExxGH.[21,22] Mutational analysis of rat DPP III has confirmed the involvement of two histidines from the HELLGH motif (residues 450−455) and Glu508 in coordination of the active-site zinc, while for Glu451 it was shown to be crucial for the catalytic activity.[23] To reveal yet unknown constituents of DPP III active site, we used bioinformatics to find the amino acid residues which are conserved in all M49 family members, and site-directed mutagenesis of human DPP III. By such combined approach, a functional role for Tyr318 and Trp300 was demonstrated in human DPP III.[24,25]

In 2008, the gene encoding yeast *Saccharomyces cerevisiae* DPP III was cloned and heterologously expressed, and the crystal structure of the yeast orthologue was solved revealing a novel protein fold – a prototype for the whole M49 family.[26] DPP III molecule is divided into two domains by a cleft containing the catalytic zinc ion. The human DPP III 3-D structure recently solved as well (PDB code: 3fvy) closely resembles that of the yeast protein (PDB code: 3csk).

Although the crystal structures of yeast and human DPPs III (both ligand-free) provided an insight into the possible catalytic mechanism, the molecular details on substrate recognition by this type of enzyme were missing.

In our previous study we investigated ligand binding to human DPP III by combining molecular docking and molecular dynamics (MD) simulations, with site-directed mutagenesis and biochemical experiments.[27] We found that evolutionary conserved His568 is crucial for the catalytic efficiency of human DPP III: its substitution with Asn resulted 1300-fold decrease of k_{cat} for the Arg_2-2NA hydrolysis in respect to the wild-type enzyme, and significantly reduced the enzyme affinity towards the competitive inhibitor Tyr-Phe-NHOH. Molecular modeling has indicated that His568 is a constituent of the S1' subsite (with 7 other amino acid residues) and a possible proton donor during hydrolysis. The same modeling study pointed out Asn406 as one out of 3 residues forming the S2 subsite which interacts with a ligand P2 residue. In order to check importance of Asn406 for the enzymatic activity of the human DPP III, we substituted this residue by site-directed mutagenesis with Gln and Ser, overexpressed and purified the mutated forms and examined their catalytic properties.

EXPERIMENTAL METHODS

Cloning and Site-directed Mutagenesis

To obtain DPP III protein with affinity C-terminal six-histidine tag, full cDNA for DPP III (2.214 kb, contained originally in the clone IRALp962E0242Q2),[24] was cloned into pET-21b vector between *NheI and XhoI* restriction sites according to procedure described earlier by Špoljarić *et al.*[25] Thus obtained wild-type expression vector was used for further mutagenesis and protein expressions.

Point mutations of the DPP III gene: N406S, and N406Q were carried out with the QuikChange II XL Site-Directed Mutagenesis kit (Stratagene, USA) by using the primers listed in Table 1. The sequencing of complete DPP III gene, as well as confirmation of each mutant, were obtained with automated sequence analyzer "ABI PRISM® 3100-Avant Genetic Analyzer" (Applied Biosystems, USA) using ABI PRISM BigDye Terminator v3.1 Ready Reaction Cycle Sequencing Kit, commercial T7 forward and T7 reverse primers, as well as the following internal DPP III primers: DPPIII271F, 5'-gcgttcctggtctatgccgcggg-3'; DPPIII521F, 5'-ggaattgtaccatggaagatgcc-3'; DPPIII521R, 5'-ggcatcttccatggtacaattcc-3'; DPPIII1261F, 5'-cgggagaagcttacctttctggagg-3'; DPPIII1614R, 5'-ccatgttgagccagttcacgtagatc-3'. All primers were custom synthesized by Invitrogen (USA).

Heterologous Expression and Purifications of Recombinant DPP III Proteins

Heterologous expression was performed as for human DPP III without His_6-tag,[25] with one modification: after induction, cells were grown overnight at 18 °C.

His_6-tagged DPP III proteins were purified by affinity chromatography on nickel-nitrilotriacetic acid agarose (Ni-NTA Agarose, Qiagen) as already described.[28]

All fractions of high purity (according to the SDS-PAGE analysis and the enzymatic activity assayed using Arg_2-2NA as substrate) were pooled and desalted on PD-10 columns (GE Healthcare) equilibrated with 20 mmol dm^{-3} Tris-HCl buffer (pH = 7.4). Purified protein preparations were stored in 15.6 mmol dm^{-3} Tris-HCl buffer (pH = 7.4) containing 22 % glycerol at −10 °C.

Protein purity was confirmed by gel electrophoresis under denaturing conditions, SDS-PAGE, carried out according to the method of Laemmli.[29]

Protein concentrations were determined using the protein-dye binding assay, with bovine serum albumin as a standard.[30]

Enzyme Activity Assay and Determination of Kinetic Parameters

The enzymatic activities of wild-type and mutant DPP III were determined by a standard assay at 37 °C with Arg_2-2NA as a substrate.[31] Kinetic parameters were determined at 25 °C and at pH = 8.6, in the presence of 50 μmol dm^{-3} $CoCl_2$ by initial rate measurements.[25]

Dixon plots were used to determine the K_i values for hydroxamate inhibitor at pH = 8.0.

BIOINFORMATIC METHODS

Similarity Search and Sequence Comparisons

Sequences of human DPP III homologs from other species were obtained by BLAST program search[32] from UniProt Knowledgebase. Multiple sequence alignment was performed using the CLUSTAL W2.[33]

COMPUTATIONAL METHODS

System Preparation. 3D structure of the mutants were derived from the model based on the crystal structure of the ligand-free human DPP III (PDB code: 3fvy).[27] Complexes between the inhibitor Tyr-Phe-NHOH and yeast DPP III were built using the crystal structure of the C130S yeast DPP III variant (PDB code: 3csk) as a template. In the models all Arg and Lys residues are positively charged (+1) and all Glu and Asp residues are negatively charged (−1), as expected at physiological (experimental) conditions. The initial protonation of the protein was determined by the program WHATIF (with a pH of 7.0), and the protonation of histidines was checked according to their ability to form hydrogen bonds with neighboring amino acid residues.

Ligands were accommodated into the wild-type proteins binding pocket using the combined approach consisting of docking by the AutoDock 4 program[34] and the steered molecular dynamics simulations (for details of the procedure see the reference 27). The complexes with the mutated proteins were built from the wild-type ones by replacing Asn406 either by Gln or Ser.

The protein parametrization was performed within the AMBER ff03 force field of Duan *et al.*,[35] while the ligands parameters were derived using Antechamber in the Amber10 program package (http://ambermd.org/). For the zinc cation, Zn^{2+}, the parameters derived in our previous work[36] and modified according to a PDB survey were used.[37]

Simulations. Simulations of the ligand-free proteins and protein-ligand complexes were performed in explicit water (TIP3P water type) using periodic boundary conditions. In order to neutralize the system Na^+ ions were placed at the protein surface, in vicinity of the charged amino acid residues. The resulting systems, consisted of ≈ 80 000 atoms (≈ 23 000 molecules of water). The electrostatic interactions were calculated using the particle-mesh Ewald method.[38,39]

Prior to molecular dynamics simulations, the protein geometry was optimized in three cycles with different constraints. In the first cycle (1500 steps), waters and substrate molecule were relaxed, while protein and zinc atom were constrained using a harmonic potential with a force constant of 133.98 kJ mol^{-1} $Å^{-2}$. In the second (2500 steps), and the third cycles (1500 steps), the same constant was applied to the zinc atom while only the protein backbone was constrained with 133.98 and 41.87 kJ $mol^{-1}Å^{-2}$, respectively. The energy minimization procedure, consisting of 470 steps of steepest descent followed by the conjugate gradient algorithm for the remaining optimization steps, was the same in all three cycles. During the first period of equilibration (100 ps of gentle heating from 0 to 300 K), the *NVT* ensemble was used. The rest of the MD simulations (water density adjustment and production simulations) were performed at constant temperature and pressure (300 K and 1 atm, the *NPT* ensemble). The temperature was held constant using Langevin dynamics with a collision frequency of 1 ps^{-1} and a time step 1 and 2 fs in the case of the human, and yeast DPP III, respectively. Bonds involving hydrogen atoms were constrained using the SHAKE algorithm. The longest were the MD simulations for the DPP III-Arg_2-2NA(RRNA) complex (30 ns), follows simulations for the yeast DPP III-Tyr-Phe-NHOH(INH) complex (2 × 20 ns), N406Q-RRNA (10 ns), N406S-RRNA (5 ns) and N406S-INH (2.5 ns).

Importantly, the octahedral coordination of the Zn cation was retained in all these complexes, except in the N406Q-RRNA complex.

The root-mean square deviation (RMSD) and root-mean square coordinate fluctuation (RMSF) of each residue in the system were calculated using the "ptraj" module of the Amber program.

MM-PBSA Calculations. The binding free energies were calculated using the Molecular Mechanics Poisson-Boltzmann Surface Area (MM-PBSA) approach[40] as implemented in the AMBER10 program.[41,42] MM-PBSA calculations were performed on the trajectory sampled during the last 5 or 2 ns of MD simulations. For this purpose snapshots were extracted from the MD trajectory every 10 ps and the binding free energies were calculated using the equation:

$$\Delta G_{\text{bind}} = G_{\text{complex}} - \left[G_{\text{protein}} + G_{\text{ligand}} \right]$$

The Gibbs free energies were approximated with the sum of conformational energy and the free energy of solvation. The polar component of desolvation free energy was calculated using the Poisson-Boltzmann method and the non-polar component was determined by $\Delta G_{\text{nonpol}} = \gamma\text{SASA} + \beta$, in which the solvent-accessible surface area (SASA) was calculated with the MolSurf program.[43] The surface tension γ and the offset β were set to the standard values of 0.02269 kJ mol^{-1} Å^{-2} and 3.85204 kJ mol^{-1}, respectively.

RESULTS AND DISCUSSION

Conservation of Asn406

Molecular modeling pointed out importance of Asn406 in human DPP III for the substrate binding.[27] To investigate the conservation of this asparagine in the metallopeptidase M49 family, we performed multiple alignments of all M49 family members sequences available in the UniProt Knowledgebase. Interestingly, it was found that this Asn is conserved in all 89 eukaryotic sequences, while all of 75 prokaryotic sequences available contained a serine residue at this position. Figure 1 illustrates this finding at reduced dataset consisting of primary structures from 14 selected species. Asparagine 406 was located in the second, starting from the N-terminus, out of 5 highly conserved regions. This result compares well with those reported by us in 2004 when altogether only 14 homologous protein sequences − members of the family M49 – were deposited in public databases.[21] However, up to now, there was no experimental evidence on the function of the conserved region 2 in proteins of DPP III family.

Expression and Purification of Wild-type and Mutated Human DPP III

In addition to conservative substitution by glutamine, asparagine at position 406 in human DPP III was replaced, using the site-directed mutagenesis, also by the serine, due to the absolute conservation of this amino acid residue in the bacterial sequences (Figure 1).

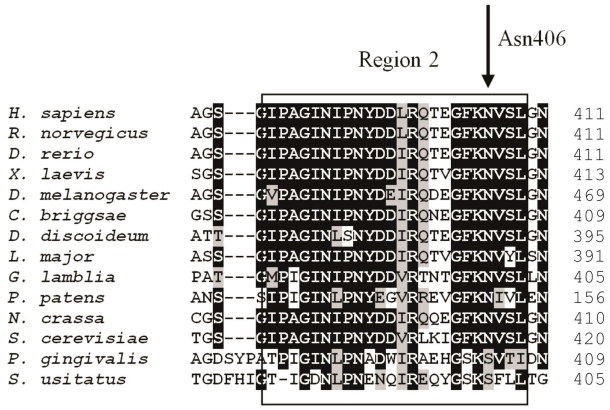

Figure 1. Conservation of Asn406 in eukaryotic sequences of family M49. Multiple sequence alignment of a selection of significantly similar peptidases of DPP III family (peptidase family M49) was obtained using CLUSTAL W2.[33] Final presentation shows partial alignment diagram of sequences: *Homo sapiens* (Q9NY33), *Rattus norvegicus* (O55096), *Danio rerio* (Q6DI20), *Xenopus laevis* (Q6PA12), *Drosophila melanogaster* (Q9VHR8), *Caenorhabditis briggsae* (A8XGF7), *Dictyostelium discoideum* (Q557H1), *Leishmania major* (Q4QJA6), *Giardia lamblia* (A8BTV2), *Physcomitrella patens subsp. patens* (A9SKT3), *Neurospora crassa* (Q7SH28), *Saccharomyces cerevisiae* (Q08225), *Porphyromonas gingivalis* (B2RLB9), and *Solibacter usitatus* (Q02C27). Residues printed in white on black are those identical in at least 12 out of 14 aligned proteins, whereas similar amino acid residues are shadowed gray. Well conserved Asn is indicated with black arrow and the highly conserved sequence region 2 is framed.

Constructs for the His-tagged DPP III, wild-type and mutants N406Q and N406S were generated and the genes were overexpressed in *E. coli* BL21(DE3)RIL$^+$ as described in the Experimental Methods section. Mutations were confirmed by DNA sequence analysis. The wild-type DPP III and mutated forms were purified by affinity chromatography on Ni-NTA agarose. Figure 2 shows the purification profile for N406S. SDS-PAGE demonstrated that the wild-type and mutant recombinant proteins appeared as bands with similar molecular mass of about 82 kDa.

Substrate Specificity towards Dipeptidyl 2-naphthylamides

Substrate specificity of His-tagged human DPP III and its variants was examined with dipeptidyl 2-naphthylamides (Table 2). Apparently the mutants N406Q and N406S similarly to the wild-type enzyme preferred Arg_2-2NA, while Ala_2-2NA was hydrolyzed

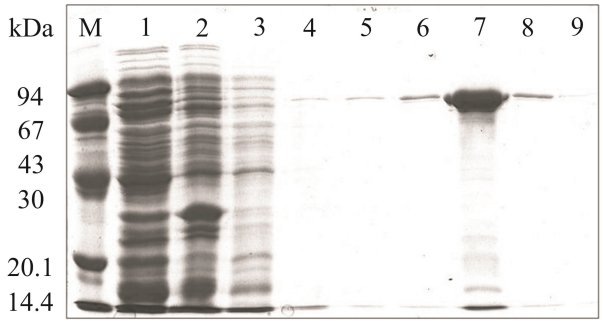

Figure 2. SDS-PAGE (10 % gel) analysis of the purification progress of human DPP III- His_6 protein (N406S mutant) by affinity chromatography on Ni-NTA agarose column. *Lanes*: *M* - protein molecular mass standards; *1* − *E. coli* cleared cell lysate containing recombinant DPP III protein; *2* − flow-through Ni-NTA column; *3*−*5* − Ni-NTA column-wash steps with 20 mmol dm^{-3} imidazole; *6*−*9* − human DPP III-His_6 protein (N406S mutant) eluted with 150 mmol dm^{-3} imidazole. Proteins were visualized by Coomassie Blue staining.

less efficiently (Table 2). This finding is in agreement with the published data on native human erythrocyte and recombinant untagged human DPP III.[25,44]

Effect of Metal Ions and Chelating Agent

Since the Zn^{2+} ion is natural cofactor of DPPs III, the influence of the zinc salt (zinc acetate) addition on the activity of all three enzyme variants was investigated. Zinc acetate was added in reaction mixture in the concentration range of 0.02 μmol dm^{-3} to 30 μmol dm^{-3}. There was no activation observed for any of the enzyme forms (wild-type human DPP III, N406S, N406Q). On the contrary, already 1 μmol dm^{-3} $Zn(Ac)_2$ inhibited all three enzymes about 30 %, and in concentration of 30 μmol dm^{-3} it caused 80 % inhibition of the wild-type DPP III, and about 95 % inhibition of both mutants.

Table 2. Substrate specificity towards dipeptidyl 2-naphthylamides

Substrate	Relative hydrolysis rate / %		
	Wild-type DPP III	N406S	N406Q
Arg-Arg-2NA	100	100	100
Ala-Ala-2NA	1.6	0.9	1.0
Gly-Pro-2NA	0	0	0
Gly-Phe-2NA	0	0	0

The enzymes were incubated at 37 °C in 50 mmol dm^{-3} Tris-HCl buffer, pH = 8.0 with 50 μmol dm^{-3} $CoCl_2$ with the substrates at a final concentration of 0.04 mmol dm^{-3}.

(100 % = 41.2 μmol or 7.9 μmol or 0.45 μmol of Arg_2-2NA hydrolyzed per min and milligram of the wild-type DPP III, N406S or N406Q, respectively).

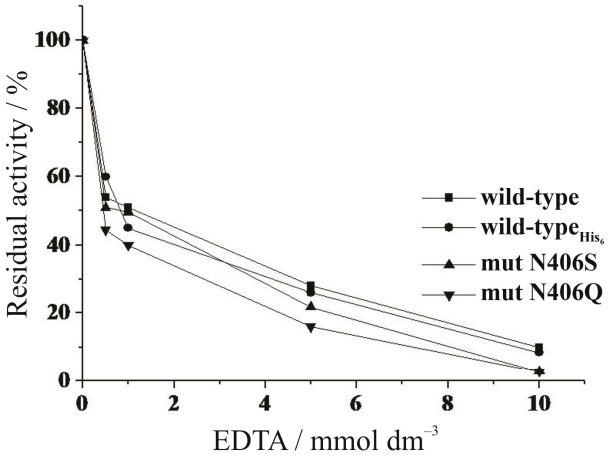

Figure 3. Effect of EDTA on the wild-type (His-tagged and untagged) and asparaginyl mutants (His-tagged) of recombinant human DPP III. The enzyme was preincubated with EDTA for 20 min at 23 °C, and the residual activity was determined at 37 °C and at pH 8.6 as described in Experimental Methods, but without the addition of metal salt ($CoCl_2$). The enzyme concentrations were: 5.8×10^{-10} mol dm^{-3} wild-type without the His-tag, 6.0×10^{-10} mol dm^{-3} wild-type His-tagged, 1×10^{-10} mol dm^{-3} N406S His-tagged, and 6.7×10^{-8} mol dm^{-3} N406Q His-tagged. The wild-type human DPP III without the His-tag was purified as described.[25]

The addition of $CoCl_2$ (5 to 200 μmol dm^{-3}) activated the wild-type DPP III and both enzyme variants, maximal activation (of about 2-fold) being at 50 μmol dm^{-3} $CoCl_2$ for all enzyme forms.

Effect of metal chelator ethylenediaminetetraacetic acid (EDTA) was examined by preincubation of the enzyme with EDTA for 20 min at 23 °C and by following the residual activity in function of the chelating agent concentration (Figure 3). A very similar inactivation profile was obtained for all enzyme forms investigated: wild-type human DPP III, wild-type His-tagged human DPP III, His-tagged mutants N406S and N406Q. Preincubation with already 0.5 mmol dm^{-3} EDTA substantially (40−55 %) decreased the enzyme activity (Figure 3).

Kinetic Characterization of Asparaginyl Mutants

Catalytic properties of His-tagged wild-type and asparaginyl mutants of human DPP III were examined using favorable synthetic substrate Arg_2-2NA, and competitive inhibitor Tyr-Phe-NHOH. Substrate hydrolysis was measured at pH 8.6 in the presence of 50 μmol dm^{-3} $CoCl_2$.

The Asn406 with Ser substitution did not change significantly K_m and k_{cat} for the Arg_2-2NA hydrolysis,

Table 3. Kinetic characterization (means ± S.E. for three separate determinations) of wild-type human DPP III and Asn406 mutants[a,b]

Enzyme form	Arg-Arg-2NA hydrolysis		Tyr-Phe-NHOH
	K_m /μmol dm^{-3}	k_{cat} /s^{-1}	K_i /μmol dm^{-3}
Wild-type	3.37 ± 1.10	14.13 ± 1.67	0.23 ± 0.03
N406S	3.99 ± 0.99	10.70 ± 0.92	0.28 ± 0.02
N406Q	5.03 ± 1.23	0.21 ± 0.02	35.89 ± 5.86

[a] The kinetic parameters K_m and k_{cat} were determined from the initial reaction rates at 25 °C and at pH 8.6 with the Arg-Arg-2NA concentrations from 2.5 to 60 μmol dm^{-3}, in the presence of 50 μmol dm^{-3} $CoCl_2$, using a Hanes plot.

[b] K_i values were determined with Arg-Arg-2NA as substrate at pH = 8.0, using Dixon plots.

neither did K_i for Tyr-Phe-NHOH, compared to the wild-type (Table 3). However, large decrease in both the binding affinity of the competitive inhibitor (156-fold higher K_i value) and in the catalytic efficiency towards Arg_2-2NA (100-fold smaller ratio k_{cat}/K_m, mostly due to the decrease in k_{cat}) was observed for the N406Q mutant (Table 3). The dissociation constant of Tyr-Phe-NHOH, K_i , determined for the wild-type human DPP III-His_6 is in very good agreement with that determined for the wild-type human DPP III without His_6-tag.[25] The k_{cat} value for the hydrolysis of Arg_2-2NA of His-tagged human DPP III does not differ significantly from the k_{cat} of its untagged counterpart (21.8 ± 2.8 s^{-1}), while K_m is somewhat lower (3.37 μmol dm^{-3} *versus* 11.6 μmol dm^{-3}).[25] Apparently, impaired catalytic efficiency of N406Q mutant and its dramatically lowered inhibitor binding affinity present experimental evidences of the Asn406 importance in human DPP III ligand binding and hydrolysis. Since the K_m is not a simple enzyme-substrate binding constant, but represents the dissociation constants for all enzyme-bound substrate species, it is not surprising that the change of K_m value does not correlate with the inhibitor binding affinity, K_i. Interestingly, the replacement of Asn406 with Ser did not influence kinetic properties of human DPP III (Table 3).

Based on the results of the kinetic investigations it is evident that the substitution of conserved Asn with either Gln or Ser did not change the enzyme preference for the synthetic substrates dipeptidyl 2-naphthylamides (Table 2).

The catalytic efficiency reduction induced by the N406Q mutation is comparable with that induced by the W300L mutation (100-fold *versus* 78-fold decrease in k_{cat}/K_m) as shown by us recently.[25] However, contribution of Asn406 to the competitive inhibitor (Tyr-Phe-NHOH) binding seems to be much more pronounced than that of the conserved Trp300, since for W300L the K_i was "only" 29-fold higher in comparison with the value determined for the wild-type.[25]

Enzymatic hydrolysis of Arg_2-2NA was measured also without the addition of metal activator ($CoCl_2$) to the reaction mixture. Again, large decrease in k_{cat} value was observed for the N406 mutant only, compared to the wild-type His-tagged human DPP III (0.06 s^{-1} *versus* 6.0 s^{-1}), while the K_m value was not changed significantly (not shown).

MD Simulations of Human DPP III-substrate Complexes

In order to explain the observed differences in the catalytic properties of two asparaginyl mutants and to understand better the Asn406 role in ligand binding and in the substrate catalysis we performed molecular dynamics simulations for N406S and N406Q mutants ligated with Arg-Arg-2NA (RRNA) substrate. Besides a short simulation was performed for the complex between the N406Q mutant and the Tyr-Phe-NHOH inhibitor. Complexes between RRNA and N406Q and N406S were simulated for 10 and 5 ns, respectively, while the N406Q - Tyr-Phe-NHOH complex was simulated for 2.5 ns at room temperature. The simulations resulted with an interesting finding on the zinc cation coordination in the complex with the less active mutant (N406Q). While in the N406S mutant, whose activity was unchanged compared to the wild-type (Table 3), the octahedral coordination of the zinc ion, determined as stable in the wild-type DPP III and its complexes,[27] was preserved during the MD simulations, in the N406Q-RRNA complex zinc was during MD simulations mostly hepta-coordinated (see Figure 4).

In addition, two hydrogen bonds, between RRNA and Glu508 and Ser504, were lost in the N406Q-substrate complex (Figure 4b). In the N406Q − inhibitor complex, the weak van der Waals (v.d.W.) interaction with Ser504 was present only during the last 0.5 ns of MD simulations, while the CH-π interaction between the inhibitor and Ser504 has not been established (Figure 4d).

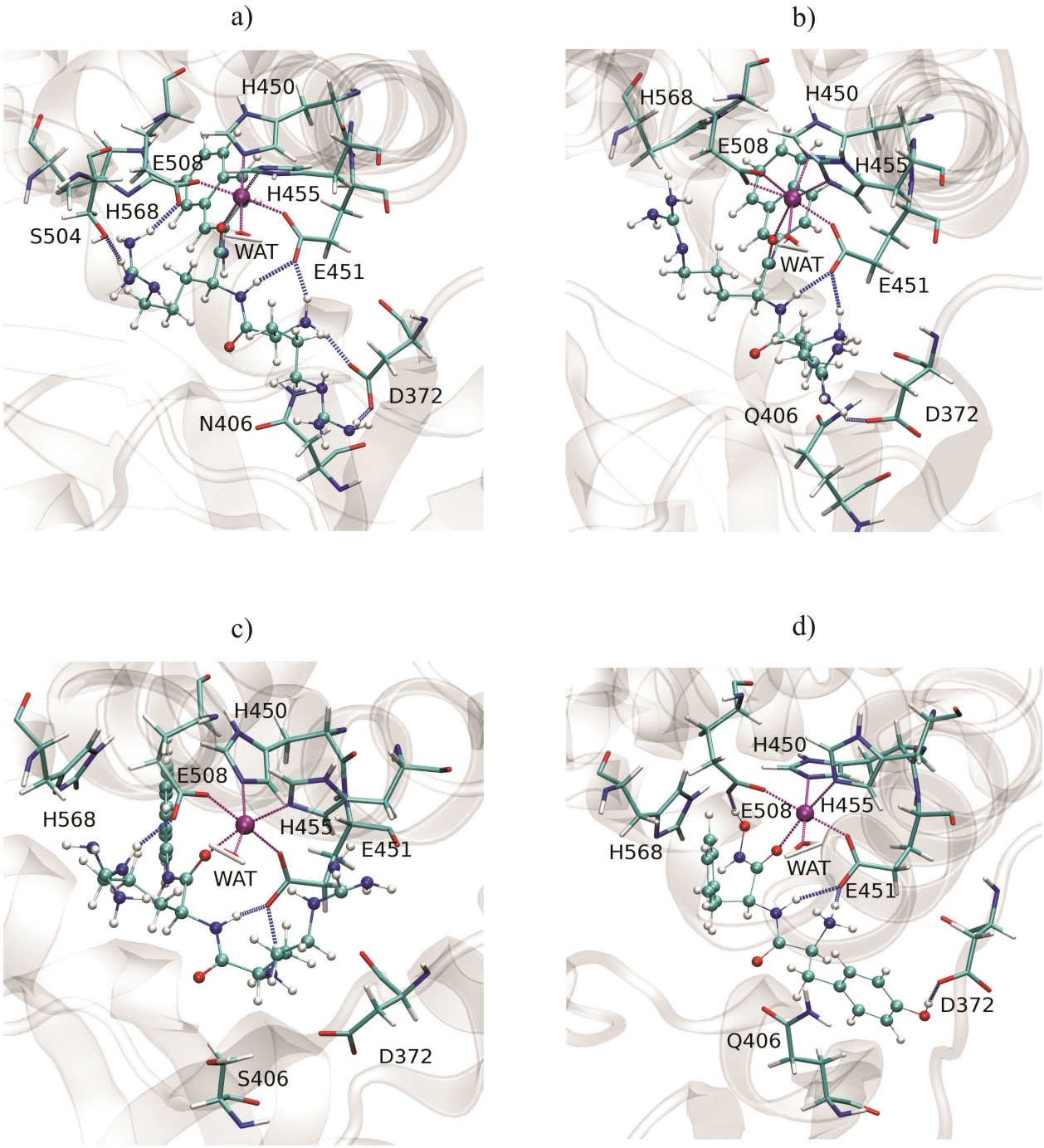

Figure 4. Coordination of the central zinc ion after: 10 ns of MD simulation for RRNA in complex with a) WT and b) N406Q mutated human DPP III, 5 ns of MD simulation for c) N406S-RRNA complex, and 2.5 ns of MD simulation for d) N406Q mutant in complex with Tyr-Phe-NHOH. The zinc cation is shown as a magenta sphere, and ligands are shown in ball and stick representation. Magenta dashed lines represent zinc coordination with electron donors, and dark blue dashed lines H-bonds that these electron donors make.

Analysis of the overall proteins flexibility showed the largest discrepancies in the calculated delta RMSF values for residues constituting the protein "lower" domain. In the complexes between RRNA and the mutated proteins the "lower" domain region, situated just below the enzyme active site, a part of which is mutated Asn406, showed increased flexibility, while the rest of the domain seemed to be less flexible. In the N406Q-RRNA complex the beta sheet from the "lower" domain (residues 388−408), just below the zinc binding site,

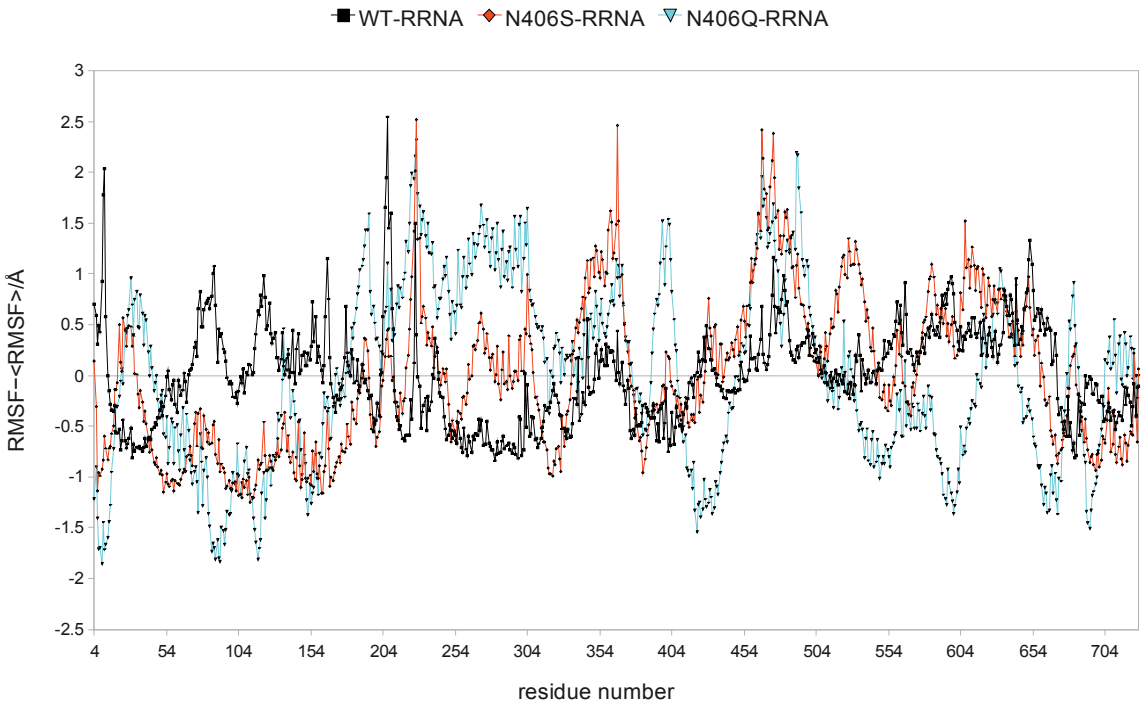

Figure 5. The delta RMSF values of the protein backbone (RMSF − <RMSF>) in wild-type and mutant's complexes with synthetic substrate for the last 5 ns and 2 ns of MD simulations, respectively. Flexible loop and α-helix connecting "lower" and "upper" domain are made by residues 337 to 374. Amino acids 424 to 666 constitute the enzyme's "upper" domain, while rest constitute the "lower" domain.

slightly moved in the direction of the upper domain. In addition, delta RMSF values revealed increased relative mobility of the helix connecting the lower and upper domain in mutated proteins, as well as increased rigidity of the "upper" domain in the N406Q mutant protein (Figure 5).

Another interesting matter noticed in the complexes with the N406Q mutant is orientation of the catalytically important His568. Actually, during MD simulations His568 is mostly in position to form a hydrogen bond with Glu512 and away from Glu508 (not shown). Apparently its suggested role in the peptide hydrolysis seems to be hindered in the mutant, and this is in agreement with the experimental findings. On the other hand, according to the MM-PBSA calculations, the substrate (RRNA) binding affinities towards the wild-type protein and mutants are practically the same, with energy difference being within the error of calculations.

MD Simulation of Yeast DPP III-inhibitor Complexes

Asn415 in the yeast DPP III corresponds to Asn406 in the human DPP III. In order to investigate if this structurally equivalent residue plays a role in the ligand binding to the yeast orthologue, we performed MD simulations for the yeast DPP III Tyr-Phe-NHOH complexes.

The inhibitor, Tyr-Phe-NHOH, was accommodated into the active site of the yeast DPP III in two different orientations. In one (complex 1) it was bound to the Zn ion by the carbonyl oxygen of the first peptide bond from the N terminus, and in the other (complex 2) by the carbonyl oxygen of the second peptide bond from the N terminus.

In the case of complex 1, Asn415 has v.d.W. interactions with the substrate N terminus, and electrostatic and CH-π interactions with its Tyr (Table 4), while in the complex 2, Asn415 interacts with both amino acid residues of the inhibitor, Tyr and Phe *via* v.d.W and electrostatic interactions (Table 5).

The binding free energy evaluated using MM-PBSA method was lower for complex 1 (−102.8 ± 14.1 kJ mol^{-1}), than for complex 2 (−46.1 ± 14.3 kJ mol^{-1}). For the inhibitor binding to the human DPP III, the evaluated binding free energy was −118.7 ± 21.6 kJ mol^{-1}. In this complex inhibitor is bound to the zinc cation by the carbonyl oxygen of the second peptide bond from the N terminus.[27]

Interestingly, MD simulations of human enzyme-ligand complexes indicated the involvement of Asn406 in the binding of the residue in P2 position (first Arg and Tyr in RRNA and Tyr-Phe-NHOH, respectively) only.[27] Considering relatively low homology between the human and yeast DPP III protein (36 % sequence

Table 4. Interactions between the wild-type yeast DPP III and inhibitor Tyr-Phe-NHOH (in complex 1)

		P1		P1`		P2`	
$^{+}H_3N$-		-Tyr-		-Phe-		-NHOH	
		S1		S1`		S2`	
Asn-415	v.d.W.	Pro-380	v.d.W. & elec.	Gly-398	CH-π	His-578	H
Glu-461	H	Asp-381[(a)]	H & elec.	Val-416 [(a)]	H		
His-465	H	Phe-413	CH-π	Ser-417	H		
		Asn-415	elec. & CH-π	Glu-517	H		
		His-465	elec. & v.d.W.				

[(a)] Hydrogen bond to the amide group

Table 5. Interactions between the wild-type yeast DPP III and inhibitor Tyr-Phe-NHOH (in complex 2)

	P2		P1		P1`	
$^{+}H_3N$-	-Tyr-		-Phe-		-NHOH	
	S2		S1		S1`	
Asn-400	CH-π & elec.	Phe-382	CH-π	Glu-517	H & elec.	
Phe-413	v.d.W.	Asn-415	v.d.W. & elec.			
Asn-415	v.d.W. & elec.	Ser-417	elec.			
		Glu-461	elec.			

identity), the different role of Asn415 in the ligand stabilization observed in the yeast complex is not surprising.

Different catalytic efficiency (k_{cat}/K_m) in the RRNA hydrolysis, the human enzyme is two orders of magnitude more efficient than the yeast DPP III, also suggests that their active sites are somewhat different.

CONCLUSIONS

Recent computational results indicated that asparagine residue in position 406 of human dipeptidyl peptidase III (737 amino acids) is a constituent of its substrate binding subsite S2.

In order to investigate the functional role of this, in all eukaryotic M49 peptidases conserved Asn, experimentally, we prepared recombinant human DPPs III (the wild-type and two mutants, N406S and N406Q), heterologously expressed them with C-terminal His_6-tag, purified and kinetically characterized.

Kinetic results obtained with the N406Q mutant support the Asn406 involvement in the ligand (competitive Tyr-Phe-NHOH peptide inhibitor) binding and substrate catalysis. However, the substitution of Asn406 with Ser did not change K_m and k_{cat} for the Arg-Arg-2NA hydrolysis, and K_i for Tyr-Phe-NHOH.

Molecular dynamics simulations performed for complexes between different enzyme forms (wild-type, N406S and N406Q) and the substrate Arg-Arg-2NA revealed the difference in the active-site zinc coordination only in the complex with the N406Q mutant. In this complex two hydrogen bonds stabilizing the substrate in the complex with the wild-type protein were lost, and the orientation of catalytically important residue His568 changed. This could impair ligand binding and catalytic efficiency of N406Q enzyme form.

In yeast DPP III, Asn415 corresponds to Asn406 in human enzyme. The importance of Asn415 for ligand binding was confirmed by MD simulations of yeast DPP III-ligand(inhibitor) complexes.

Acknowledgements. Support for this study by the Croatian Ministry of Science, Education and Sport (Projects 098-1191344-2938, 098-0982913-2829 and 098-1191344-2860) is gratefully acknowledged.

REFERENCES

1. J. K. McDonald and A. J. Barrett (Eds.), *Mammalian Proteases: A Glossary and Bibliography, Exopeptidases*, Vol. 2, Academic Press, London, 1986, pp. 127−131.
2. J.-M. Chen and A. J. Barrett, *Dipeptidyl-peptidase III*, in: A. J. Barrett, N. D. Rawlings, and J. F. Woessner (Eds.), *Handbook of Proteolytic Enzymes*, Second ed.,Vol. 1, Elsevier, Amsterdam, 2004, pp. 809−812.

3. S. Ellis and J. M. Nuenke, *J. Biol. Chem.* **242** (1967) 4623−4629.
4. Y. Shimamori, Y. Watanabe, and Y. Fujimoto, *Chem. Pharm. Bull.* **34** (1986) 3333−3340.
5. M. Abramić, M. Zubanović, and Lj. Vitale, *Biol. Chem. Hoppe-Seyler* **369** (1988) 29−38.
6. T. Vanha-Perttula, *Clin. Chim. Acta* **177** (1988) 179−196.
7. E. Kecorius, D. H. Small, and B. G. Livett, *J. Neurochem.* **50** (1988) 38−44.
8. K. R. Lyn, *Int. J. Biochem.* **23** (1991) 47−50.
9. C.-M. Lee and S. H. Snyder, *J. Biol. Chem.* **257** (1982) 12043−12050.
10. M. Smyth and G. Ocuinn, *J. Neurochem.* **63** (1994) 1439−1445.
11. I. Ohkubo, Y.-H. Li, T. Maeda, Y. Yamamoto, T. Yamane, P.-G. Du, and K. Nishi, *Biol. Chem.* **380** (1999) 1421−1430.
12. J. Huang, J. Kim, P. Ramamurthy, and T. H. D. Jones, *Exp. Mycol.* **16** (1992) 102−109.
13. Y. Watanabe, Y. Kumagai, and Y. Fujimoto, *Chem. Pharm. Bull.* **38** (1990) 246−248.
14. T. Chiba, Y.-H. Li, T. Yamane, O. Ogikubo, M. Fukuoka, R. Arai, S. Takahashi, T. Ohtsuka, I. Ohkubo, and N. Matsui, *Peptides* **24** (2003) 773−778.
15. M. Baršun, N. Jajčanin, B. Vukelić, J. Špoljarić, and M. Abramić, *Biol. Chem.* **388** (2007) 343−348.
16. Š. Šimaga, D. Babić, M. Osmak, J. Ilić-Forko, Lj. Vitale, D. Miličić, and M. Abramić, *Eur. J. Cancer* **34** (1998) 399−405.
17. Š. Šimaga, D. Babić, M. Osmak, M. Šprem, and M. Abramić, *Gynecol. Oncol.* **91** (2003) 194−200.
18. H. Zhang, Y. Yamamoto, S. Shumiya, M. Kunimatsu, K. Nishi, I. Ohkubo, and K. Kani, *Histochem. J.* **33** (2001) 511−521.
19. M. Yang, H. S. Lee, and M.Y. Pyo, *Environ. Mol. Mutagen.* **49** (2008) 368−373.
20. K. Fukasawa, K. M. Fukasawa, M. Kanai, S. Fujii, J. Hirose, and M. Harada, *Biochem. J.* **329** (1998) 275−282.
21. M. Abramić, J. Špoljarić, and Š. Šimaga, *Period. Biolog.* **106** (2004) 161−168.
22. N. D. Rawlings, F. R. Morton, C. Y. Kok, J. Kong, and A. J. Barrett, *Nucleic Acids Res.* **36** (2008) D320−D325.
23. K. Fukasawa, K. M. Fukasawa, H. Iwamoto, J. Hirose, and M. Harada, *Biochemistry* **38** (1999) 8299−8303.
24. B. Salopek-Sondi, B. Vukelić, J. Špoljarić, Š. Šimaga, D. Vujaklija, J. Makarević, N. Jajčanin, and M. Abramić, *Biol. Chem.* **389** (2008) 163−167.
25. J. Špoljarić, B. Salopek-Sondi, J. Makarević, B. Vukelić, D. Agić, Š. Šimaga, N. Jajčanin-Jozić, and M. Abramić, *Bioorg. Chem.* **37** (2009) 70−76.
26. P. Kumar Baral, N. Jajčanin-Jozić, S. Deller, P. Macheroux, M. Abramić, and K. Gruber, *J. Biol. Chem.* **283** (2008) 22 316−22 324.
27. A. Tomić, M. Abramić, J. Špoljarić, D. Agić, D. M. Smith, and S. Tomić *J. Mol. Recogn.* **24** (2011) 804−814.
28. N. Jajčanin-Jozić, S. Deller, T. Pavkov, P. Macheroux, and M. Abramić, *Biochimie* **92** (2010) 89−96.
29. U. K. Laemmli, *Nature* **227** (1970) 680−685.
30. M. M. Bradford, *Anal. Biochem.* **72** (1976) 248–254.
31. M. Abramić, Š. Šimaga, M. Osmak, L. Čičin-Šain, B. Vukelić, K. Vlahoviček, and Lj. Dolovčak, *Int. J. Biochem. Cell Biol.* **36** (2004) 434−446.
32. S. F. Altschul, T. L. Madden, A. A. Schäffer, J. Zhang, Z. Zhang, W. Miller, and D. Lipman, *Nucleic Acids Res.* **25** (1997) 3389−3402.
33. M. A. Larkin, G. Blackshields, N. P. Brown, R. Chenna, P. A. McGettigan, H. McWilliam, F. Valentin, I. M. Wallace, A. Wilm, J. D. Thompson, T. J. Gibson, and D. G. Higgins, *Bioinformatics* **23** (2007) 2947−2948.
34. G. Morris, D. Goodsell, R. Halliday, R. Huey, W. Hart, R. K. Belew, and A. J. Olson, *J. Computat. Chem.* **19** (1999) 1639−1662.
35. Y. Duan, C. Wu, S. Chowdhury, M. C. Lee, G. Xiong, W. Zhang, R. Yang, P. Cieplak, R. Luo, T. Lee, J. Caldwell, J. Wang, and P. Kollman, *J. Computat. Chem.* **24** (2003) 1999−2012.
36. B. Bertoša, B. Kojić-Prodić, R. Wade, and S. Tomić, *Biophys. J.* **94** (2008) 27−37.
37. I. Dokmanić, M. Šikić, and S. Tomić, *Acta Cryst. D* **64** (2008) 257−263.
38. T. Darden, D. York, and L. Pedersen, *J. Chem. Phys.* **98** (1993) 10089−10092.
39. U. Essmann, L. Perera, M. L. Berkowitz, T. Darden, H. Lee, and L. G. Pedersen, *J. Chem. Phys.* **103** (1995) 8577−8592.
40. J. M. Swanson, R. H. Henchman, and J. A. McCammon, *Biophys. J.* **86** (2004) 67−74.
41. D. A. Case, T. E. III Cheatham, T. A. Darden, H. Gohlke, R. Luo, K. M. Jr. Merz, A. Onufriev, C. Simmerling, B. Wang, and R. J. Woods, *J. Computat. Chem.* **26** (2005) 1668−1688.
42. D. A. Case, T. A. Darden, T. E. III Cheatham, C. L. Simmerling, J. Wang, R. E. Duke, R. Luo, M. Crowley, R. C. Walker, W. Zhang, K. M. Merz, B. Wang, S. Hayik, A. Roitberg, G. Seabra, I. Kolossváry, K. F. Wong, F. Paesani, J. Vanicek, X. Wu, S. R. Brozell, T. Steinbrecher, H. Gohlke, L. Yang, C. Tan, J. Mongan, V. Hornak, G. Cui, D. H. Mathews, M. G. Seetin, C. Sagui, V. Babin, and P. A. Kollman, *AMBER 10*, University of California, San Francisco, 2008.
43. M. L. Connolly, *J. Appl. Cryst.* **16** (1983) 548−558.
44. M. Abramić, D. Schleuder, Lj. Dolovčak, W. Schröder, K. Strupat, D. Šagi, J. Peter-Katalinić, and Lj. Vitale, *Biol. Chem.* **381** (2000) 1233−1243.